Global model of Ar, O2, Cl2, and Ar/O2 highdensity plasma discharges

C. Lee and M. A. Lieberman

Global model of Ar, O$_2$, Cl$_2$, and Ar/O$_2$ high-density plasma discharges

C. Lee
Department of Chemical Engineering, University of California, Berkeley, California 94720

M. A. Lieberman
Department of Electrical Engineering and Computer Sciences, University of California, Berkeley, California, 94720

We develop a global (volume averaged) model of high-density plasma discharges in molecular gases. For a specified discharge length and diameter, absorbed power, pressure, and feed gas composition, as well as the appropriate reaction rate coefficients and surface recombination constants, we solve the energy and particle balance equations to determine all species densities and the electron temperature. We use an expression for charged particle diffusive loss that is valid for low and high pressures and for electropositive and electronegative plasmas. We apply the model to Ar, O$_2$, Cl$_2$, and Ar/O$_2$ discharges and compare with available experimental data. In Ar, we find that the ion density increases monotonically with increasing pressure, while for O$_2$ and Cl$_2$, the total positive ion density increases initially, then decreases as pressure is further increased. For a pure Cl$_2$ discharge, we find that surface recombination processes are important in affecting the degree of dissociation and the negative-ion density of the system. For mixtures of Ar and O$_2$, we find that at a fixed ratio of Ar to O$_2$ flowrates, the dominant ionic species changes from Ar$^+$ to O$^+$ as pressure is increased. When a small amount of Ar is added to a pure O$_2$ discharge, the overall positive-ion density increases, whereas the ratio of negative ion to electron density decreases. © *1995 American Vacuum Society.*

I. INTRODUCTION

Molecular gases and their mixtures are used in the microelectronics industry for processing steps such as thin-film etching and deposition. More specifically, electronegative gases such as chlorine and chlorine-containing mixtures are used for etching polysilicon, silicon oxide, and aluminum. The gas chemistry of these discharges, however, is poorly understood. Modeling of the plasma chemistry of electronegative discharges has been mainly in the intermediate pressure regime of several hundred mTorr to 1 Torr in parallel plate rf reactors.[1–6] Recently, Bassett and Economou[7] studied the effect of chlorine addition to an argon discharge; the model conditions, however, remained in the range of 0.3–1 Torr. Vender *et al.*[8] have measured and modeled negative-ion densities in an oxygen discharge, along with work done by Stoffels *et al.*[9] to study the ion kinetics in discharges of Ar/CF$_4$ and Ar/CCl$_2$F$_2$. The pressure ranges in these studies were between 5 and 200 mTorr; however, the discharge used was a capacitively coupled rf plasma.

High-density discharges such as radio-frequency (rf) driven transformer-coupled-plasma (TCP) sources are becoming more preferable than conventional parallel plate reactors for ultralarge scale integrated circuit processing. These discharges typically operate at low pressures of 1–20 mTorr and high input powers of 1–3 kW. The power absorption in a TCP source is typically inductive, as compared to the capacitive power absorption in an rf parallel plate reactor. Differences in the operating conditions between capacitively and inductively coupled sources can lead to drastically different behaviors in the plasma chemistry. For example, high-density discharges can be highly dissociated, hence decreasing the negative-ion concentration in the plasma by depleting the molecular source for negative-ion formation. In this article, we examine a volume-averaged (global) model of the plasma chemistry of some molecular gases and their mixtures, and compare this model to that of a pure argon discharge. A generalized power balance expression is developed that can be easily extended to include mixtures and polyatomic gases. The power balance includes energy-loss channels for electron–neutral collisions such as rotational, vibrational, and electronic excitation, dissociation, ionization, dissociative attachment, and electron detachment. In addition, energy-loss processes for heavy particle collisions such as asymmetric charge exchange and ion-ion recombination are included. Particle balances are written for all species of interest. For the charged particles, the appropriate ambipolar diffusion rates in the presence of negative ions are used to determine the positive-ion losses. The complete set of equations is solved self-consistently to obtain all species concentrations and the electron temperature.

II. MODEL FORMULATION

A. Assumptions

The cylindrical reactor geometry chosen was based on that of a commercially available TCP reactor, with $L = 7.5$ cm and $R = 15.25$ cm [Fig. 1(a)]. Assumptions of the model are listed below.

(1) All densities n are assumed to be volume averaged, i.e.,

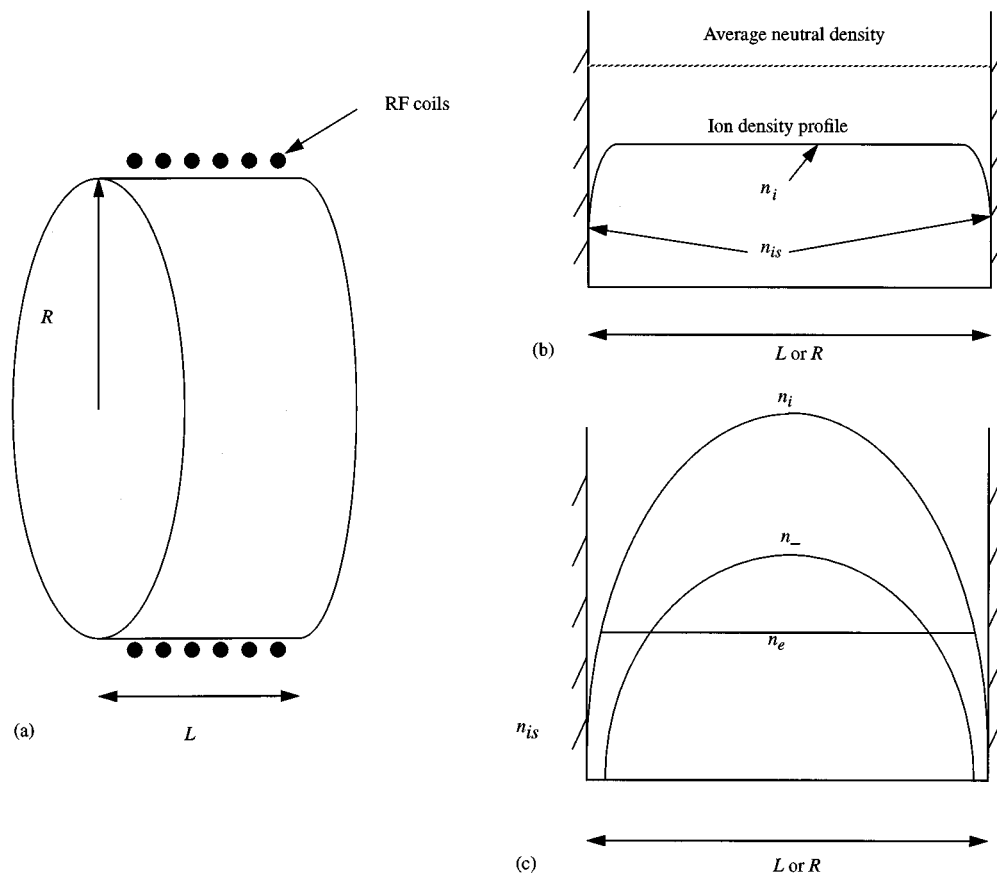$$n = \frac{1}{\pi R^2 L} 2\pi \int_0^R r\,dr \int_0^L n(r,z)\,dz.$$

FIG. 1. Description of model: (a) schematic of reactor geometry used in the model, (b) density profiles for an electropositive discharge, (c) density profiles for an electronegative discharge.

(2) For an electropositive discharge, as shown in Fig. 1(b), the positive-ion densities are assumed to have a uniform profile throughout the discharge except near the wall, where the density is assumed to drop sharply to a sheath-edge density n_{is}.

(3) For an electronegative discharge, as shown in Fig. 1(c), the electron density n_e is assumed to be uniform throughout the discharge except near the sheath edge. The negative-ion density n_- is assumed to be parabolic, dropping to zero at the sheath edge, the positive-ion density is $n_i = n_e + n_-$, with $n_i = n_e = n_{is}$ at the sheath edge. An appropriate interpolation between electropositive and electronegative profiles is used, as described in the Appendix. The relationship between the bulk positive-ion density n_i and the edge density n_{is} is discussed later in this section and in the Appendix.

(4) We neglect the energy losses for processes in which one ion is dissociated to form another and we neglect energy losses due to collisions of electrons with positive or negative ions, because in the regime of interest, the charged particle densities are small compared to the neutral densities.

(5) We neglect electron dissociation of molecular ions in the particle balance because in high-density sources, the molecular ion density is small.[10]

(6) We assume only one type of negative ion is generated.

(7) The factors h_L and h_R are assumed to be independent of the type of ions, i.e., the ion-neutral mean-free path λ is identical for all species in the discharge.

(8) The ion temperature T_i is assumed to be 0.5 eV for pressures less than 1 mTorr; for higher pressures, $T_i - T_0$ is allowed to decrease at a rate proportional to $1/p$, ultimately reaching the thermal temperature of $T_0 = 600$ K. The neutral temperature was assumed to be 600 K.

B. Generalized power balance

Two main sets of equations are used in the global model: power balance and particle balance for all species of interest. For a monatomic gas, the equations are straightforward, as discussed by Lieberman and Gottscho.[11] For an argon discharge, ignoring the presence of metastables, the electron temperature (T_e, in units of eV) is simply a function of the pressure and geometry of the system, the plasma density is proportional to the input power, and the collisional energy loss per electron–ion pair created (ϵ_L, in units of eV) is a function of T_e only. For molecular gases, the situation is

more complicated. As we will see, the plasma composition, i.e., ion and neutral densities, plays an important role in determining the electron temperature and ϵ_L.

The total power balance has the general form of

$$P_{abs} = P_{ev} + P_{iw} + P_{ew}, \tag{1}$$

where P_{abs} is the power absorbed by the system, P_{ev} is the electron energy loss due to all electron–neutral collision processes in the volume, P_{iw} is the ion energy loss to the walls, and P_{ew} is the electron energy loss to the walls. For an atomic gas, the energy loss ϵ_L per electron–ion pair created due to all electron neutral collision processes can be expressed as

$$\nu_{iz}\epsilon_L = \nu_{iz}\epsilon_{iz} + \sum_{k=1}^{N_{exc}} \nu_{exc,k}\epsilon_{exc,k} + \nu_{elas}\frac{3T_e}{2}\frac{2m}{M}, \tag{2}$$

where $\nu = \langle\sigma\nu\rangle n_n$ is the appropriate collision frequency, $\langle\sigma\nu\rangle$ is the rate coefficient, n_n is the neutral density, and N_{exc} is the number of excitation energy-loss channels. The first term on the right-hand side of Eq. (2) is the energy loss due to the ionization of neutral atoms with an ionization potential of ϵ_{iz} (in units of eV), the second term represents the total energy loss due to excitation of neutral atoms to various excited states with threshold energies ϵ_{exc}, and the last term is the energy loss due to electron–neutral elastic scattering. If we divide Eq. (2) by ν_{iz}, we obtain

$$\epsilon_L = \epsilon_{iz} + \sum_{k=1}^{N_{exc}} \frac{\nu_{exc,k}}{\nu_{iz}}\epsilon_{exc,k} + \frac{\nu_{elas}}{\nu_{iz}}\left(\frac{3mT_e}{M}\right). \tag{3}$$

Since the ratios of collision frequencies are equal to the corresponding ratios of rate constants independent of the atomic gas density, ϵ_L is a function of T_e only.

Ion energy is lost to the wall at a characteristic velocity which is the Bohm velocity $u_B = (eT_e/M)^{1/2}$, with $e = 1.6 \times 10^{-19}$ C,

$$P_{iw} = e n_s u_B A \epsilon_{iw}, \tag{4}$$

where n_s is the ion sheath edge density, A is the surface area of the chamber walls, and ϵ_{iw} is the ion kinetic energy lost per ion lost to the wall, which is typically between 5 and $8T_e$ for high-density sources; the electron energy lost to the wall has the form

$$P_{ew} = e n_{es} u_B A \epsilon_{ew}, \tag{5}$$

where $\epsilon_{ew} = 2T_e$ is the electron kinetic energy lost per electron lost to the walls.

For molecular gases, several complications can arise: (i) generation of multiple positive ions are possible; (ii) fragmentation of the neutral molecule can provide multiple neutral molecule sources for generation of ions; (iii) generation of negative ions is possible; and (iv) additional energy-loss channels such as dissociation, and particle-loss channels such as volume positive-negative ion recombination, need to be included. These factors require modification of Eqs. (1) and (2). We rewrite Eq. (1) as

$$P_{abs} = \sum_{i=1}^{r} P_{iw,i} + P_{ev} + P_{ew}, \tag{6}$$

where r is the number of positive-ion species generated in the system, i.e., for O₂, $r=2$, for generation of both O_2^+ and O^+. Equation (2) is modified to be

$$\nu_{iz,i}\epsilon_{L,i} = \sum_{j=1}^{N_{s,i}} \left(\nu_{iz,ij}\epsilon_{iz,ij} + \sum_{k=1}^{N_{exc,j}} \nu_{exc,kj}\epsilon_{exc,kj} \right.$$
$$\left. + \nu_{elas,j}\frac{2m}{M_j}\frac{3T_e}{2} \right), \tag{7}$$

where $N_{s,i}$ is the number of neutral species that generates the ith ion. For Ar^+, $N_{s,i}=2$ (Ar and Ar*); for O^+, $N_{s,i}=2$ (O and O*); for O_2^+, $N_{s,i}=1$ (O₂); for Cl^+, $N_{s,i}=1$ (Cl); and for Cl_2^+, $N_{s,i}=1$ (Cl₂). We have not included O_2^* in $N_{s,i}$ because a previous study showed that the O_2^* concentration is much lower than that of the atomic species.[10] In Eq. (7), $\nu_{iz,ij}$ is the ionization frequency for production of the ith ion from neutral species j, $\nu_{iz,i}$ is the total ionization frequency for production of the ith ion, $\epsilon_{iz,ij}$ is the threshold ionization energy for production of the ith ion from neutral species j, $\epsilon_{exc,kj}$ is the threshold excitation energy for the kth level of the jth neutral, and $\epsilon_{L,i}$ is the total collisional energy loss per electron-ion pair created for the ith ion. The sum over k includes all inelastic electron–neutral collisional processes that do not produce positive ions; e.g., rotational, vibrational and electronic excitation, dissociation, attachment, and detachment.

Dividing Eq. (7) by $\nu_{iz,i}$, $\epsilon_{L,i}$ can be expressed as

$$\epsilon_{L,i} = \frac{1}{\nu_{iz,i}} \sum_{j=1}^{N_{s,i}} \left(\nu_{iz,ij}\epsilon_{iz,ij} + \sum_{k=1}^{N_{exc,j}} \nu_{exc,kj}\epsilon_{exc,kj} \right.$$
$$\left. + \frac{\nu_{elas,j} 3mT_e}{M_j} \right). \tag{8}$$

An average energy-loss factor ϵ_L can also be defined for complicated gases and mixtures:

$$\epsilon_L \sum_{i=1}^{r} \nu_{iz,i} = \sum_{i=1}^{r} \epsilon_{L,i}\nu_{iz,i}.$$

From Eq. (8), we can see that once there are multiple sources for generating the same ion, $\epsilon_{L,i}$ is no longer a function of T_e only, but is also a function of the neutral composition in the plasma. The right-hand side of Eq. (8) includes only the possible channels for electron energy loss; electrons can also gain energy through collisions. For example, in the case of argon, metastables (Ar*) are known to be destroyed by superelastic quenching,[12–15]

$$e_{cold} + Ar^* \rightarrow e_{hot} + Ar.$$
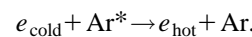
In this situation, an extra term is added to the right-hand side (rhs) of Eq. (8),

TABLE I. Oxygen reaction set.

Reaction			Rate coefficients	Reference
$e + O_2$	$\longrightarrow$	$O_2^+ + 2e$	$k_1 = 9.0 \times 10^{-10} \, (T_e)^2 \exp(-12.6/T_e) \, \mathrm{cm^3 \, s^{-1}}$	10
$e + O_2$	$\longrightarrow$	$O(^3P) + O(^1D) + e$	$k_2 = 5.0 \times 10^{-8} \exp(-8.4/T_e) \, \mathrm{cm^3 \, s^{-1}}$	10
$e + O_2$	$\longrightarrow$	$O(^3P) + O^-$	$k_3 = 4.6 \times 10^{-11} \exp(2.91/T_e - 1.26/T_e^2 + 6.92/T_e^3) \, \mathrm{cm^3 \, s^{-1}}$	10
$e + O(^3P)$	$\longrightarrow$	$O^+ + 2e$	$k_4 = 9.0 \times 10^{-9} \, (T_e)^{0.7} \exp(-13.6/T_e) \, \mathrm{cm^3 \, s^{-1}}$	10
$O^- + O_2^+$	$\longrightarrow$	$O(^3P) + O_2$	$k_5 = 1.4 \times 10^{-7} \, \mathrm{cm^3 \, s^{-1}}$	10
$O^- + O^+$	$\longrightarrow$	$O(^3P) + O(^3P)$	$k_6 = 2.7 \times 10^{-7} \, \mathrm{cm^3 \, s^{-1}}$	10
$e + O^-$	$\longrightarrow$	$O(^3P) + 2e$	$k_7 = 1.73 \times 10^{-7} \exp(-5.67/T_e + 7.3/T_e^2 - 3.48/T_e^3) \, \mathrm{cm^3 \, s^{-1}}$	10
$e + O_2$	$\longrightarrow$	$O(^3P) + O(^3P) + e$	$k_8 = 4.23 \times 10^{-9} \exp(-5.56/T_e) \, \mathrm{cm^3 \, s^{-1}}$	10
$e + O(^3P)$	$\longrightarrow$	$O(^1D) + e$	$k_9 = 4.47 \times 10^{-9} \exp(-2.286/T_e) \, \mathrm{cm^3 \, s^{-1}}$	10
$O(^1D) + O_2$	$\longrightarrow$	$O(^3P) + O_2$	$k_{10} = 4.1 \times 10^{-11} \, \mathrm{cm^3 \, s^{-1}}$	10
$O(^1D) + O(^3P)$	$\longrightarrow$	$O(^3P) + O(^3P)$	$k_{11} = 8.1 \times 10^{-12} \, \mathrm{cm^3 \, s^{-1}}$	10
$O(^1D)$	$\xrightarrow{\text{(wall)}}$	$O(^3P)$	$k_{12} = D_{\mathrm{eff}}/\Lambda^2 \, \mathrm{s^{-1}}$	10
$e + O(^1D)$	$\longrightarrow$	$O^+ + 2e$	$k_{13} = 9.0 \times 10^{-9} \, (T_e)^{0.7} \exp(-11.6/T_e) \, \mathrm{cm^3 \, s^{-1}}$	a
$O^+(g)$	$\xrightarrow{\text{(wall)}}$	$O(^3P)(g)$	$k_{14} = 2u_{B,O^+}(R^2 h_L + RL h_R)/R^2 L \, \mathrm{s^{-1}}$	b
$O_2^+(g)$	$\xrightarrow{\text{(wall)}}$	$O_2(g)$	$k_{15} = 2u_{B,O_2^+}(R^2 h_L + RL h_R)/R^2 L \, \mathrm{s^{-1}}$	b
$O(g)$	$\xrightarrow{\text{(wall)}}$	$\frac{1}{2}O_2(g)$	$k_{16} = \gamma_{\mathrm{rec}} D_{\mathrm{eff}}/\Lambda^2 \, \mathrm{s^{-1}}$	
$T_e[=] \mathrm{eV}$				

[a]This rate coefficient is estimated from k_4, where the same process takes place except that the threshold is 13.6 eV instead of 11.6 eV.
[b]These surface loss rate coefficients are estimated from the diffusion of ions to the walls (see the Appendix).

$$\epsilon_{\mathrm{gain}} = \left(-\frac{1}{\nu_{\mathrm{iz},i}} \right) \nu_q \epsilon_q ,$$

where ν_q is the de-excitation frequency and ϵ_q is the energy gained per collision.

Using the continuity equation for the ith positive ion, including volume losses due to positive–negative ion recombination and asymmetric charge exchange (for the case of mixtures), we have

$$Vn_e \nu_{\mathrm{iz},i} = A n_{is} u_{B,i} + V k_{\mathrm{rec},i} n_i n_- + V \sum_{j=1}^{N_s} k_{\mathrm{cx},ij} n_i n_j , \qquad (9)$$

where V is the reactor volume, $k_{\mathrm{rec},i}$ is the recombination rate coefficient, $k_{\mathrm{cx},ij}$ is the charge-exchange rate coefficient for

asymmetric collisions between the ith ion and the jth neutral, and n_- is the negative-ion density. The last term on the RHS of Eq. (9) is the loss of the ith ion through collisions with the jth neutral to generate another ionic species, hence, for the ion that is generated from the jth neutral, the asymmetric charge exchange reaction will appear as a generation term in the particle balance equation rather than a loss term. The densities at the sheath edge are related by the quasineutrality condition,

$$n_{es} = \sum_{i=1}^{r} n_{is} , \qquad (10)$$

and the total power lost in the volume is

TABLE II. Chlorine reaction set.

Reaction			Rate coefficients	Reference
$e + Cl_2$	$\longrightarrow$	$Cl_2^+ + 2e$	$k_1 = 9.21 \times 10^{-8} \exp(-12.9/T_e) \, \mathrm{cm^3 \, s^{-1}}$	34
$e + Cl_2$	$\longrightarrow$	$Cl^+ + Cl + 2e$	$k_1 = 3.88 \times 10^{-9} \exp(-15.5/T_e) \, \mathrm{cm^3 \, s^{-1}}$	34
$e + Cl_2$	$\longrightarrow$	$Cl^+ + Cl^- + e$	$k_1 = 8.55 \times 10^{-10} \exp(-12.65/T_e) \, \mathrm{cm^3 \, s^{-1}}$	34
$e + Cl_2$	$\longrightarrow$	$2Cl(^2P) + e$	$k_2 = 3.80 \times 10^{-8} \exp(-3.824/T_e) \, \mathrm{cm^3 \, s^{-1}}$	35
$e + Cl_2$	$\longrightarrow$	$Cl(^2P) + Cl^-$	$k_3 = 3.69 \times 10^{-10} \exp(-1.68/T_e + 1.457/T_e^2 - 0.44/T_e^3 + 0.0572/T_e^4 - 0.0026/T_e^5) \, \mathrm{cm^3 \, s^{-1}}$	34
$e + Cl(^2P)$	$\longrightarrow$	$Cl^+ + 2e$	$k_4 = (T_e/12.96)^{0.5} \exp(-12.96/T_e)(1.419 \times 10^{-7} - 1.864 \times 10^{-8} \log(T_e/12.96) - 5.439 \times 10^{-8} \log(T_e/12.96)^2 + 3.306 \times 10^{-8} \log(T_e/12.96)^3 - 3.54 \times 10^{-9} \log(T_e/12.96)^4 - 2.915 \times 10^{-8} \log(T_e/12.96)^5) \, \mathrm{m^3 \, s^{-1}}$	31
$Cl^- + Cl_2^+$	$\longrightarrow$	$Cl(^2P) + Cl_2$	$k_5 = 5.0 \times 10^{-8} \, \mathrm{cm^3 \, s^{-1}}$	6
$Cl^- + Cl^+$	$\longrightarrow$	$Cl(^2P) + Cl(^2P_u)$	$k_6 = 5.0 \times 10^{-8} \, \mathrm{cm^3 \, s^{-1}}$	6
$e + Cl^-$	$\longrightarrow$	$Cl(^2P) + 2e$	$k_7 = 2.63 \times 10^{-8} \exp(-5.37/T_e) \, \mathrm{cm^3 \, s^{-1}}$	32
$Cl(^2P)$	$\longrightarrow$	$1/2 \, Cl_2$	$k_{12} = \gamma_{\mathrm{rec}} D_{\mathrm{eff}}/\Lambda^2 \, \mathrm{s^{-1}}$	10
Cl^+	$\longrightarrow$	$Cl(^2P)$	$k_{14} = 2u_{B,Cl^+}(R^2 h_L + RL h_R)/R^2 L \, \mathrm{s^{-1}}$	a
Cl_2^+	$\longrightarrow$	$Cl_2(g)$	$k_{15} = 2u_{B,Cl_2^+}(R^2 h_L + RL h_R)/R^2 L \, \mathrm{s^{-1}}$	a
$T_e[=] \mathrm{eV}$				

[a]These surface loss rate coefficients are estimated from the diffusion of ions to the walls (see the Appendix).

TABLE III. Argon reaction set.

Reaction			Rate coefficients	Reference
$e+Ar$	$\longrightarrow$	$Ar^+ + 2e$	$k_1 = 1.23 \times 10^{-7} \exp(-18.68/T_e)$ cm^3 s^{-1}	26
$e+Ar$	$\longrightarrow$	$Ar^* + e$	$k_2 = 3.71 \times 10^{-8} \exp(-15.06/T_e)$ cm^3 s^{-1}	27
$e+Ar^*$	$\longrightarrow$	$Ar^+ + 2e$	$k_3 = 2.05 \times 10^{-7} \exp(-4.95/T_e)$ cm^3 s^{-1}	25
$e+Ar^*$	$\longrightarrow$	$Ar+e$	$k_4 = 2.0 \times 10^{-7}$ cm^3 s^{-1}	12–14
$Ar^* + Ar^*$	$\longrightarrow$	$Ar + Ar^+$	$k_5 = 6.2 \times 10^{-10}$ cm^3 s^{-1}	12–14
Ar^+	$\longrightarrow$	Ar	$k_6 = 2u_{B,Ar^+}(R^2 h_L + R L h_R)/R^2 L$ s^{-1}	a
Ar^*	$\longrightarrow$	Ar	$k_7 = D_{eff}/\Lambda^2$ s^{-1}	10
$T_e[=]$ eV				

^{a}These surface loss rate coefficients are estimated from the diffusion of ions to the walls (see the Appendix).

$$P_{ev} = e n_e V \sum_{i=1}^{r} \nu_{iz,i} \epsilon_{L,i}. \tag{11}$$

Substituting Eq. (10) into Eq. (5), and Eq. (9) into Eq. (11), the total power balance of Eq. (6) becomes

$$P_{abs} = \sum_{i=1}^{r} e n_i \left(A_{eff} \epsilon_{T,i} u_{B,i} + k_{rec,i} n_- \epsilon_{L,i} V \right.$$
$$\left. + \sum_{j=1}^{N_s} k_{cx,ij} n_j \epsilon_{L,i} V \right), \tag{12}$$

in which A_{eff} is the effective surface area for ion loss,[11]

$$A_{eff} = \left. \frac{n_{is}}{n_i} \right|_{axial} 2\pi R^2 + \left. \frac{n_{is}}{n_i} \right|_{radial} 2\pi R L,$$

and

$$\epsilon_{T,i} = \epsilon_{L,i} + \epsilon_{iw} + \epsilon_{ew}.$$

The ratio of sheath edge density n_{is} to the bulk average density n_i is derived in the Appendix and is found to be

$$h_L = \left. \frac{n_{is}}{n_i} \right|_{axial} = \frac{1 + 3\alpha_{avg}/\gamma}{1 + \alpha_{avg}} \frac{0.86}{[3 + L/2\lambda + (0.86 L u_B/\pi D_a)^2]^{1/2}}, \tag{13}$$

at the axial sheath edge ($z=0$ and $z=L$) and

$$h_R = \left. \frac{n_{is}}{n_i} \right|_{radial} = \frac{1 + 3\alpha_{avg}/\gamma}{1 + \alpha_{avg}} \frac{0.8}{(4 + R/\lambda + \{0.8 R u_B/2.405[J_1(2.405)D_a]\}^2)^{1/2}}, \tag{14}$$

at the radial sheath edge ($r=R$). Here $\alpha_{avg} = n_-/n_e$ is the ratio of negative ion to electron density, $\gamma = T_e/T_i$, λ is the ion-neutral mean-free path, D_a is the ambipolar diffusion coefficient, and J_1 is the Bessel function of the first order. The assumptions stated earlier about h_L and h_R mean that the ion-neutral momentum transfer cross sections are independent of the type of ion or neutral present in the plasma. For the systems we are interested in studying, this assumption is reasonable because the difference in atomic sizes for the neutrals is at the most a factor of 2, i.e., O$_2$ vs O, or Cl vs Cl$_2$, leading to approximately the same factor of difference in the ion-neutral collision cross sections. Furthermore, since at the low pressures of interest we are taking the square root of λ in Eqs. (13) and (14), the error introduced by small differences in λ is small. The terms in Eqs. (13) and (14) involving the ambipolar diffusion coefficient $D_a \sim e T_e/M_i \nu_i$, with $\nu_i = \nu_{thi}/\lambda$ and ν_{thi} the ion thermal velocity, are important only at the highest pressures of interest. In calculating ν_{thi}, the assumption of ion temperature T_i being 0.5 eV is valid for

pressures less than 1 mTorr;[16,17] for higher pressures, $T_i - T_0$ is allowed to decrease at a rate proportional to $1/p$, ultimately reaching the thermal temperature of $T_0 = 0.052$ eV.

C. Discharges of argon, oxygen, and chlorine

The generalized electron power balance obtained in Eq. (12) enables us to study complicated gases and mixtures. We have applied the formulation to systems of atomic and molecular gases. The reaction sets used for Ar, O$_2$, and Cl$_2$ and the excitation processes are listed in Tables I–V. Excitation processes for O$_2$ can be found in a previous publication.[10] Types of electron–neutral reactions included are ionization, dissociation, excitation, dissociative excitation, dissociative attachment, and electron detachment. Dissociative ionization of molecular gas is not included for two reasons: (1) the threshold for this process is higher, and hence the reaction probability is low; (2) the density of molecular species is low due to the high dissociation rate, hence decreasing the overall rate of reaction. We have verified this by running the

TABLE IV. Energy-loss reactions for chlorine molecules.

Reaction		Rate coefficient	Reference
$e + Cl_2$ ⟶	$Cl_2(b^3\Pi_u) + e$	$k = -6.13 \times 10^{-10} \exp(2.74/T_e - 6.85/T_e^2 + 3.69/T_e^3$ $0.856/T_e^4 + 0.0711/T_e^5)$ cm^3 s^{-1}	32
⟶	$Cl_2(^1\Pi_u) + e$	$k = 3.80 \times 10^{-8} \exp(-3.824/T_e)$ cm^3 s^{-1}	32
⟶	$Cl_2(^1\Pi_g) + e$	$k = 9.74 \times 10^{-9} \exp(-10.71/T_e)$ cm^3 s^{-1}	32
⟶	$Cl_2(^1\Sigma_u) + e$	$k = 2.12 \times 10^{-9} \exp(-11.16/T_e)$ cm^3 s^{-1}	32
⟶	$Cl_2 + e$	$k = 4.47 \times 10^{-7} \exp(-2.17/T_e + 0.362/T_e^2 - 0.0196/T_e^3)$ cm^3 s^{-1} (momentum transfer)	32
⟶	$Cl_2^+ + e$	$k = 9.21 \times 10^{-8} \exp(-12.9/T_e)$ cm^3 s^{-1}	34
⟶	$Cl_2 + e$	$k = 9.26 \times 10^{-10} \exp(5.85/T_e - 4.94/T_e^2 + 1.716/T_e^3 - 0.251/T_e^4 + 0.123/T_e^5)$ cm^3 s^{-1} (vibrational excitation)	32
⟶	$2Cl(^2P) + e$	$k = 3.80 \times 10^{-8} \exp(-3.824/T_e)$ cm^3 s^{-1}	35

simulation with and without the dissociative ionization process, and found no significant difference in the results. Three-body recombination reactions are not included since at the pressure range of interest, i.e., less than 100 mTorr, the rate coefficients are orders of magnitude smaller compare to other processes. Ion–ion and neutral–neutral interactions are also included through the processes of positive-negative ion recombination and metastable quenching. Two-step ionization, i.e., excitation from the ground to a metastable state, followed by ionization from the metastable state, are included for Ar and O₂. We did not include metastables for the chlorine discharge, since metastables were found to be unimportant in contributing to the total positive-ion density in O₂ discharges due to their low concentration,[10] and the threshold energy (10 eV) required for the generation of Cl* is much larger than that of O* (2 eV). Chlorine metastables, presumably will have the same generation and loss mechanisms as that of O*, hence, we concluded that Cl* is unimportant. For argon, the largest loss rate of Ar* was through superelastic quenching by cold electrons. Unlike oxygen, quenching of Ar* by ground-state Ar is not an efficient process due to the lack of vibrational and rotational energy levels in the atomic gas.[12–14] Besides volume quenching, we have also included wall quenching, in which metastable species are de-excited upon striking the chamber walls, and the ground-state species are returned to the reactor. This process is controlled by diffusion; hence the loss rate to the wall is largest at low pressure. The diffusional losses are represented in Tables I–V by $k \sim D_{eff}/\Lambda^2$, where D_{eff} is the effective diffusion coefficient of the neutral species of interest,[11] which has the expression

$$D_{eff} = \frac{1}{(1/D_{AA*} + 1/D_{KN})},$$

where D_{AA*} is the diffusion coefficient estimated using the Chapman–Enskog equation for gas diffusivity,[18] and D_{KN} is the Knudsen free-diffusion coefficient equal to $\nu_{th}\Lambda/3$, Λ is the effective diffusion length given by

$$\frac{1}{\Lambda^2} = \left(\frac{\pi}{L}\right)^2 + \left(\frac{2.405}{R}\right)^2,$$

and $\nu_{th} = (kT_0/M)^{1/2}$ is the neutral thermal velocity. The types of reactions used for Cl₂ are identical to those of O₂, with the exclusion of metastables. The difference in the chemical nature of chlorine and oxygen, however, can lead to different results. For example, the bond strengths of Cl₂ and O₂ are 2.5 and 5.5 eV, respectively. The weaker chlorine bond generates more Cl under the same process conditions, therefore decreasing the concentration of negative ions in the discharge through depletion of the Cl₂ source density for Cl⁻ production by electron attachment. The more electronegative nature of chlorine, however, tends to increase the Cl⁻ density because of a larger attachment rate coefficient to Cl₂. We will see the influence of these competing effects in Sec. III.

The continuity equations for the neutrals is written based on the mass conservation principal of generation rate=loss rate. Details of the individual terms included for each type of mechanism can be found in Ref. 10.

D. Mixtures of argon and oxygen

The chemistry of the discharge is complicated when mixtures are considered. Most processing discharges use mixtures of two or more gases in order to achieve the desired etch profile, selectivity, and etch rate. We choose to study a mixture of argon and oxygen. The chemistry of this system allows us to capture some effects of gas mixtures on the discharge parameters. The reactions that describe the interac-

TABLE V. Energy-loss reactions for chlorine atoms.

Reaction		Process	Reference
$e + Cl(^2P)$ ⟶	$Cl(^3D) + e$	$k = 1.99 \times 10^{-8} \exp(-10.06/T_e)$ cm^3 s^{-1}	33
⟶	$Cl(^4D) + e$	$k = 9.24 \times 10^{-9} \exp(-11.15/T_e)$ cm^3 s^{-1}	33
⟶	$Cl(^4P) + e$	$k = 1.60 \times 10^{-8} \exp(-10.29/T_e)$ cm^3 s^{-1}	32
⟶	$Cl(^4S) + e$	$k = 1.27 \times 10^{-8} \exp(-10.97/T_e)$ cm^3 s^{-1}	33
⟶	$Cl(^5D) + e$	$k = 5.22 \times 10^{-9} \exp(-11.12/T_e)$ cm^3 s^{-1}	33
⟶	$Cl(^5P) + e$	$k = 2.79 \times 10^{-9} \exp(-11.06/T_e)$ cm^3 s^{-1}	32

TABLE VI. Argon–oxygen reactions.

Reaction			Rate coefficients	Reference
$O^- + Ar^+$	$\longrightarrow$	$Ar + O$	$k = 2.70 \times 10^{-7}$ cm³ s⁻¹	a
$O_2 + Ar^*$	$\longrightarrow$	$Ar + O_2$	$k = 1.12 \times 10^{-9}$ cm³ s⁻¹	b
$O + Ar^*$	$\longrightarrow$	$Ar + O$	$k = 8.10 \times 10^{-12}$ cm³ s⁻¹	b
$O_2 + Ar^*$	$\longrightarrow$	$Ar + O + O$	$k = 5.80 \times 10^{-11}$ cm³ s⁻¹	c
$O_2 + Ar^+$	$\longrightarrow$	$O_2^+ + Ar$	$k = 1.20 \times 10^{-11}$ cm³ s⁻¹	38
$O + Ar^+$	$\longrightarrow$	$O^+ + Ar$	$k = 1.20 \times 10^{-11}$ cm³ s⁻¹	d

[a]The reaction rate was assumed to be identical to the O^-/O^+ recombination rate.
[b]Estimated from similar quenching reactions for Cl₂ and N₂ give in Refs. 13 and 14.
[c]Estimated from similar reactions in NH₃ given in Ref. 39.
[d]Estimated to be the same as the O_2/Ar^+ reaction obtained from Ref. 38.

tion between argon and oxygen are listed in Table VI. The presence of Ar^+ can act as an additional loss channel for negative ions through ion–ion recombination, and Ar^* can be de-excited by both neutral O_2 and O. We have not considered Penning ionization, i.e., ionization of neutral species by metastables, since neither Ar^* nor O^* has enough energy to overcome the ionization thresholds of O_2, O, and Ar. We have, however, included dissociation of O_2 by metastable argon. Nonresonant exothermic charge exchange was also included, in which Ar^+ is charge exchanged with O_2 and O; the reverse reactions were not considered because the energies carried by O_2^+ and O^+, 12.6 and 13.6 eV, respectively, are not sufficient to ionize Ar, whose ionization potential is 15.6 eV.

III. RESULTS AND DISCUSSION

Equation (12) for power balance is solved simultaneously with particle balances for each species, and charge neutrality is used to obtain the electron density. The pressure of the system is calculated based on neutrals only, with $p = \Sigma n_j kT$, where n_j is the jth neutral species and T is the neutral temperature. Input parameters for the model are power, inlet pressure, which is determined from density of the feed gas Cl_2; flowrate, composition of the neutral feed gas, and surface recombination coefficient γ_{rec} for O or Cl. The inlet pressure is defined as the pressure when the discharge is off,

and hence is based on the density of the neutral feed gas only. Unless otherwise indicated, the results presented in this paper are at a fixed absorbed power of 1000 W and total flowrate of 35 sccm. Pressure, feed gas composition, and γ_{rec} are varied, and their effects on fractional dissociation, electronegativity, and plasma composition are studied. In this section, we first describe the differences between atomic and molecular gases. Next we compare the two different molecular gases, and finally, we present results for a mixture of atomic and molecular gases.

A. Atomic and molecular gases

A major difference between atomic and molecular gases is the availability of energy-loss channels. Electrons, upon colliding with neutral atoms/molecules, can lose energy and excite the heavy particle into an electronically, vibrationally, or rotationally excited state. For an atomic gas, there are no vibrational or rotational states available. Hence the collisional energy lost per electron–ion pair created ϵ_L is much less for a monatomic gas than for a diatomic gas, especially at low electron temperatures, where ϵ_L is dominated by excitation losses (see Fig. 2).

Figure 3 shows the electron temperature dependence on pressure for pure Ar, O_2, and Cl_2 discharges. The trends are similar, with T_e decreasing with increase pressure. The difference in the values of T_e demonstrates that the electron temperature is a function of the plasma composition. Under identical operating conditions, we see that T_e can differ by
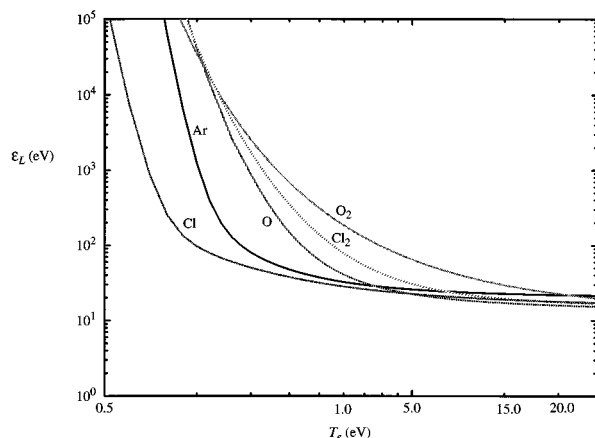

FIG. 2. Collisional energy loss per electron–ion pair created vs T_e. Note differences between molecular gases of O_2, Cl_2, and atomic species Ar, O, and Cl.
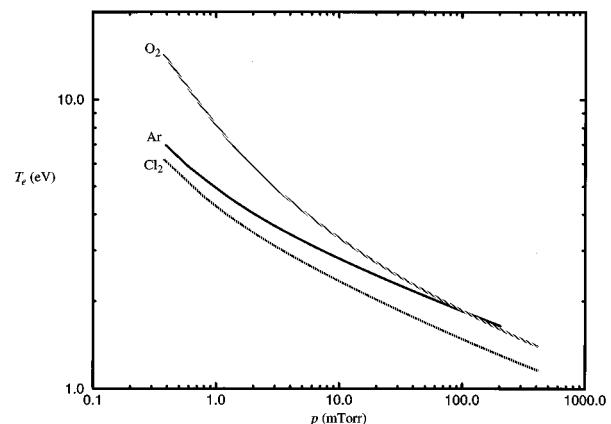

FIG. 3. Electron temperature T_e vs pressure for the three systems of Ar, O_2, and Cl_2. Absorbed power = 1000 W, $Q = 35$ sccm, $\gamma_{rec} = 0.0$.
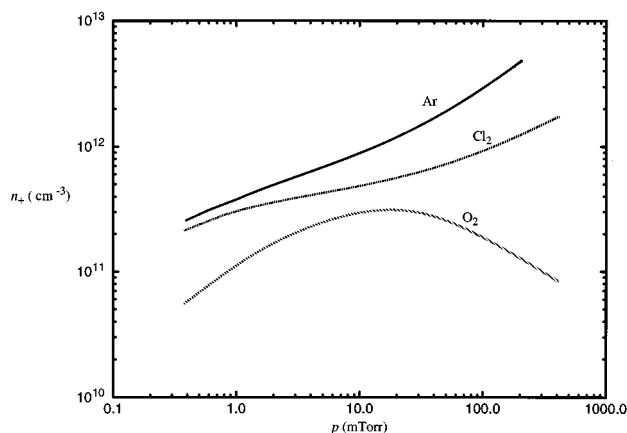
FIG. 4. Total positive-ion density n_+ vs pressure. Conditions are the same as Fig. 2.

up to a factor of 2 or more, especially in the lower-pressure range. The difference is due to the fact that T_e is determined from the particle balances,[11] and because we have included balances for both neutral and charged species, T_e is determined by the dominant ion/neutral component of the discharge. Depending upon the species present in the greatest amount, T_e will vary accordingly. The total positive-ion density for the three systems is presented in Fig. 4. An argon discharge consistently has the highest density for the entire pressure range studied. The molecular gases are at lower densities, with oxygen having the lowest overall n_+. The differences in the ion densities are due to the factors of ϵ_L and A_{eff} in Eqs. (8) and (12). From Eq. (8), one can see that the electron energy loss is directly proportional to the number of available energy-loss channels of the neutral species; hence, ϵ_L for argon is much less than ϵ_L for oxygen and chlorine, since there are fewer energy-loss channels for the atomic gas. The effective loss area A_{eff} is a decreasing function of pressure because the ions are more confined at higher pressures. The energy loss factor ϵ_L, on the other hand, increases with increasing p. Comparing the effects of ϵ_L and A_{eff} in Eq. (12), we can see that as the pressure increases, the two factors vary in opposite directions. Whichever factor dominates will determine the behavior of the total positive-ion density with pressure. From Fig. 4, one can conclude that at a fixed power, for Ar and Cl₂, A_{eff} decreases faster than the increase in ϵ_L as pressure increases, with the overall result that the ion density increases; for oxygen, however, n_+ increase initially but decreases at higher pressures, which points to the dominance of ϵ_L over A_{eff}.

B. Oxygen and chlorine discharges

For molecular gases, surface recombination processes can be important, especially if the atom of interest has a high surface recombination coefficient,[19] as is believed to be the case of Cl. This reaction is the recombination of a gaseous atom with an adsorbed atom on the reactor wall, using the wall surface as a third body:
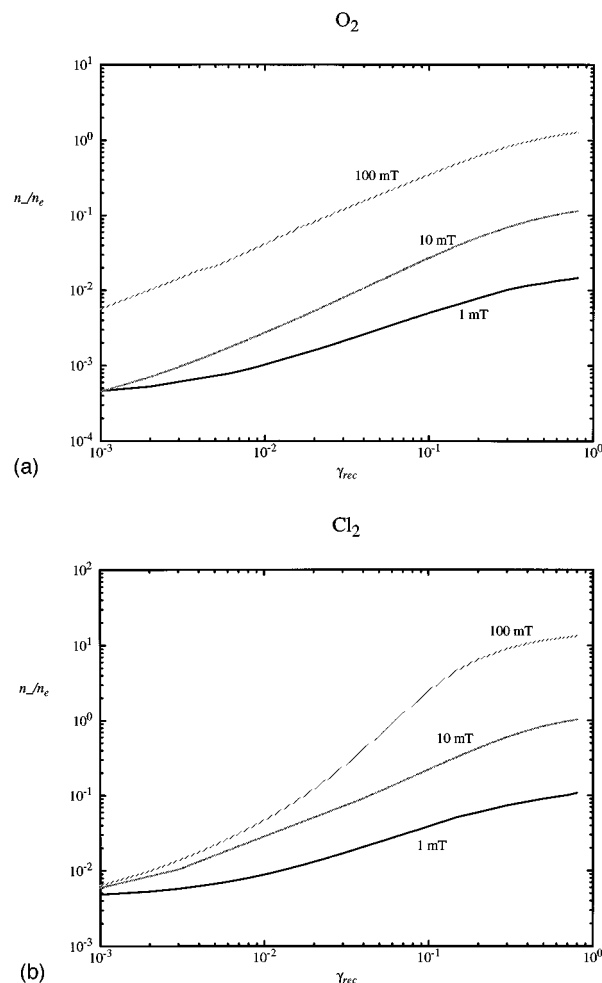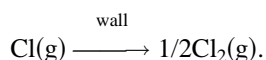
$$Cl(g) \xrightarrow{\text{wall}} 1/2 Cl_2(g).$$

FIG. 5. (a) Ratio n_-/n_e of negative ions to electrons vs γ_{rec} for an oxygen discharge. Absorbed power = 1000 W, Q = 35 sccm. (b) Ratio n_-/n_e of negative ions to electrons vs γ_{rec} for a chlorine discharge. Conditions are the same as (a).

This provides an additional source for Cl₂, which enhances the electronegativity of the plasma. The Cl₂ bond is weak, however, and the molecule can be dissociated, regenerating Cl and decreasing the negative-ion concentration. These two competing effects strongly depend on the recombination coefficient γ_{rec}, as shown in Fig. 5. The ratio of n_-/n_e is plotted against γ_{rec} with pressure as a parameter for discharges of pure O₂ and Cl₂. From Fig. 5(a), we can see that the recombination coefficient does not have a major effect on the electronegativity of O₂; n_-/n_e approaches unity at $\gamma_{rec} = 0.4$ and a pressure of 100 mTorr. Note that this value of γ_{rec} suggests that four out of every ten oxygen atoms that strike the wall will recombine to form O₂. This is unlikely, because the surface recombination coefficient for oxygen on a clean surface is reported to be $\sim 10^{-4}$.[20] For a surface that is passivated with oxygen, the recombination coefficient is even lower due to the low physisorption surface coverage. For Cl₂, however, the situation is different. Chlorine is believed to have a high γ_{rec}, which has made it difficult for researchers to measure the Cl atom concentration in the afterglows of discharges.[21] Values of γ_{rec} reported in literature have been as high as 0.15.[19] Furthermore, chlorine is more electronega-
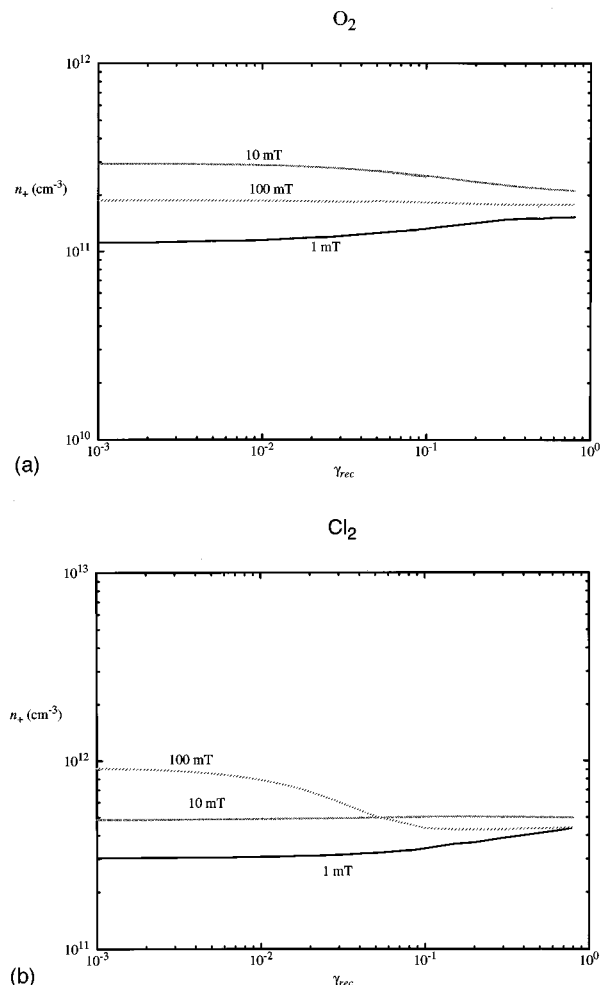
FIG. 6. (a) Total positive-ion density n_+ vs γ_{rec} for O$_2$. Conditions are the same as Fig. 5(a). (b) Total positive-ion density n_+ vs γ_{rec} for Cl$_2$. Conditions are the same as Fig. 5(a).

FIG. 7. (a) Fractional dissociation vs γ_{rec} for O$_2$. Conditions are the same as Fig. 5(a). (b) Fractional dissociation vs γ_{rec} for Cl$_2$. Conditions are the same as Fig. 5(a).

tive than oxygen, and therefore, has a greater tendency to form negative ions due to the higher reaction probability or attachment rate. From Fig. 5(b), we see that the negative-ion density exceeds the electron density at $\gamma_{rec}=0.08$ at a pressure of 100 mTorr. Interpolating between the 10 and 100 mTorr curves at $\gamma_{rec}=0.1$, it is not difficult to see that negative ions can become important in the operating range of high-density sources (1–20 mTorr). The difference in n_-/n_e for O$_2$ and Cl$_2$ is consistent with the chemical nature of the two gases, with chlorine being a more electronegative gas and Cl$^-$ having a higher electron affinity than O$^-$, 3.62 vs 1.45 eV, respectively.

The effect of γ_{rec} on the total positive-ion density n_+, is presented in Fig. 6. Figure 6(a) shows that for an oxygen discharge, surface recombination has little effect on the total positive ion density. For the range of γ_{rec} investigated, the variation of n_+ does not differ much compare to the $\gamma_{rec}=0$ case (see Fig. 4); for chlorine, however, Fig. 6(b) shows that surface recombination decreases n_+ as γ_{rec} becomes greater than 0.05 in the high-pressure regime. In this situation, Cl$^+$ is no longer the dominant positive ion, and the densities of the two types of positive ions, Cl$^+$ and Cl$_2^+$, are comparable in magnitude. The decrease in n_+ is due to the increase in the
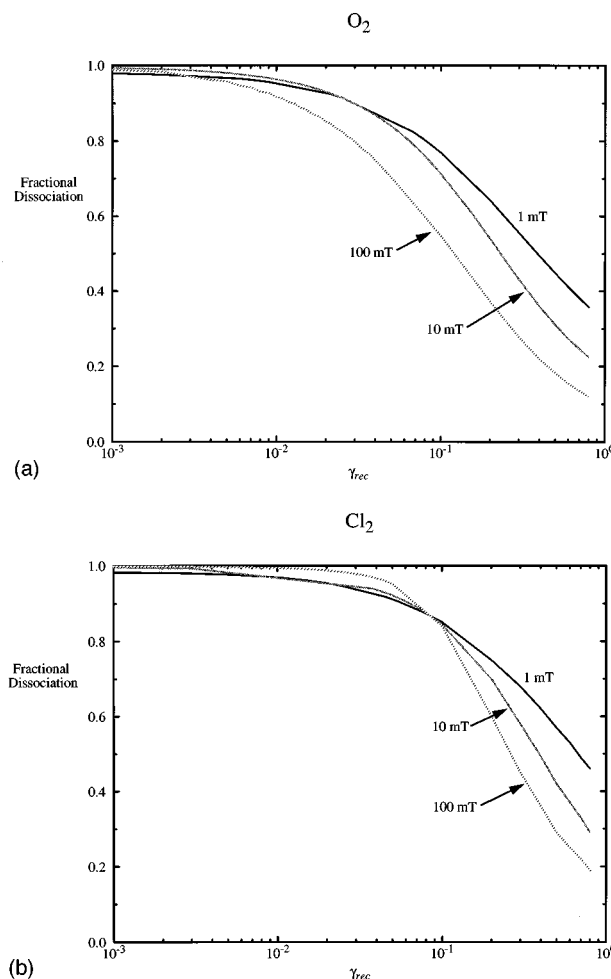
energy-loss factor ϵ_L. Recall from Sec. II that the ion density is strongly affected by the collisional energy loss per electron–ion pair created, and since ϵ_L for Cl$_2$ much exceeds ϵ_L for Cl, the total ion density drops as a result. The electron temperature, T_e, is also affected by γ_{rec} through the enhancement in electronegativity. The results show that at high pressures, T_e ($\gamma_{rec}=0.1$)$>T_e(\gamma_{rec}=0)$ for both O$_2$ and Cl$_2$ due to the increase in the negative ion density. As n_- increases, n_e drops, hence the electron temperature must rise to sustain the required ionization rate.[10]

An additional variable that is of concern for high-density discharges is the fractional dissociation of the neutral feed gas, which is defined as the ratio of the density of the atomic neutral, O or Cl, to the total neutral density. A high degree of dissociation will result in a high concentration of reactive-free radicals which can directly influence process output parameters such as the etch rate. Figures 7(a) and 7(b) show the effect of γ_{rec} on discharges of O$_2$ and Cl$_2$ for pressures of 1, 10, and 100 mTorr. For a large γ_{rec}, the fractional dissociation decreases as expected, since neutral atoms are depleted through wall recombination to generate neutral molecules. For the case of $\gamma_{rec}=0.1$, Cl$_2$ is ~80% dissociated, whereas O$_2$ is ~50% dissociated; the difference in fractional disso-
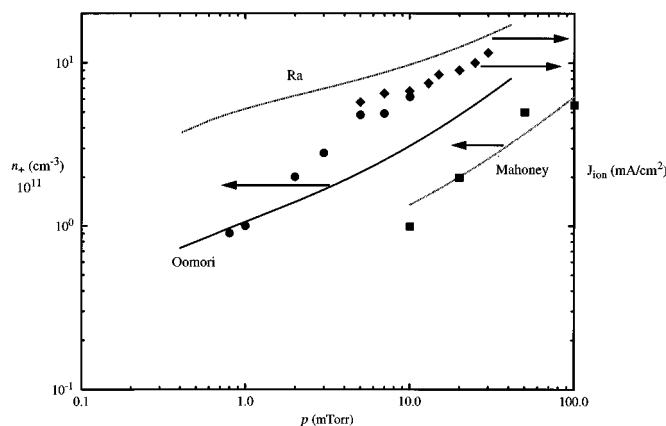
FIG. 8. Comparison with experimental data for argon discharges. Curves are model results based on corresponding operating conditions and reactor geometry. Ra et al. (Ref. 22) (--- model, ◆ experiment); Mahoney et al. (Ref. 23) (--- model, ■ experiment); Oomori et al. (Ref. 24) (— model, ● experiment).

ciation is partly due to the difference in bond strengths of each molecule, which is directly related to the collision cross section of the dissociation process; and the difference in electron temperatures. The double bond in the oxygen molecule makes it more difficult to dissociate O₂ than Cl₂, which has a single bond. The bond energies are 5.5 vs 2.5 eV, respectively; hence, under identical operating conditions, the fractional dissociation of O₂ is lower than that of Cl₂. Note that the dependence of fractional dissociation on γ_{rec} is highly nonlinear. No significant changes in fractional dissociation are observed until $\gamma_{rec} > 0.02$.

C. Comparison with experimental data

Model results for both Ar and Cl₂ are compared with available experimental data. Oxygen result comparisons were discussed in a previous publication[10] and are not included here. Figures 8 and 9 are comparisons of the total positive ion density versus pressure for Ar and Cl₂, respectively. In both figures, the symbols are the experimental data,
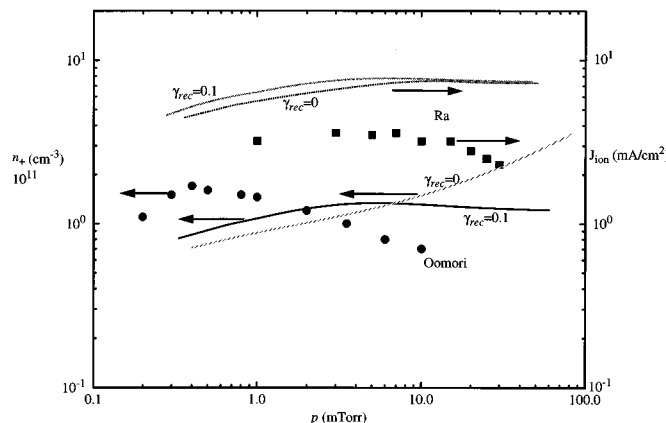

FIG. 9. Comparison with experimental data for chlorine discharges. Curves are model results based on corresponding operating conditions and reactor geometry. Ra et al. (Ref. 22) (--- model, $\gamma_{rec}=0$, --- model, $\gamma_{rec}=0.1$, ■ experiment); Oomori et al. (Ref. 24) (--- model, $\gamma_{rec}=0$, — model, $\gamma_{rec}=0.1$, ● experiment).

and the curves are the model results. In Fig. 8, Ra et al.[22] (◆ symbol) gave values of ion current density in a TCP system rather than ion density, hence, we calculated J_{ion} using the expression $J_{ion}=en_+u_B$. Data from Mahoney et al.[23] (■) were also obtained in a TCP system, whereas Oomori et al.[24] (●) took measurements in an extended ECR source. For all three cases, the experimental data show that the Ar⁺ density increases monotonically with increasing pressure, which agrees qualitatively with values predicted by the model.

For a pure chlorine discharge, ion densities were measured by Ra et al. and Oomori et al. The results are presented in Fig. 9 (■ Ra et al.; ● Oomori et al.). Both sets of experimental results show that the total positive-ion density decreases slightly as the pressure is increased. The model predictions for J_{ion} show that the effect of γ_{rec} is small, and only small percentage differences were observed in the low-pressure range of 0.2–5 mTorr. On the other hand, the model predictions for the ion density in the Oomori system show a significant dependence on γ_{rec}. For $\gamma_{rec}=0$, n_+ steadily increases with increasing p, but with $\gamma_{rec}=0.1$, n_+ increases initially and then decreases at higher pressures, which follows the experimental trend. The difference between the two sets of experimental data is due to the difference in the operating conditions and the geometry of the systems. In the ECR system, the volume is much larger and the flowrate is low (10 sccm), hence the residence time is long. In the TCP, however, the volume is 13 times smaller, and there is a higher flowrate of 80 sccm. This difference in residence times leads to significantly different ion compositions for the two systems, and hence a significantly different sensitivity to surface recombination processes. This change in the trend of n_+/J_{ion} vs p shows the importance of reactor geometry, operating conditions, and the strong coupling to surface reactions, which can affect the overall positive-ion density.

D. Mixtures of argon and oxygen

When argon is added to an oxygen discharge, the discharge becomes complicated. There are three types of positive ions, O₂⁺, O⁺, Ar⁺, and five different neutrals, O₂, O, O*, Ar, Ar*, in addition to negative (O⁻) ions and electrons. The interactions between these species are listed in Table VI. The total flowrate into the system is held fixed at 35 sccm, and the composition of the feed gas is varied to achieve a desired argon to oxygen ratio. The fraction of Ar (f_{Ar}) used in Figs. 10 and 11 is defined as the ratio of Ar flowrate to the total neutral flowrate. The pressure is varied from 1 to 50 mTorr. The fraction of ions that are Ar⁺ is plotted in Fig. 10 as a function of f_{Ar}. At a fixed feed gas composition, for example, $f_{Ar}=0.5$, the fraction of Ar⁺ decreases with increasing pressure. At 1 mTorr, Ar⁺ makes up more than 50% of the total positive-ion density, whereas at 50 mTorr, less than 30% of the positive ions are Ar⁺. This dependence on pressure can be explained through the difference in the ionization rate coefficients for O⁺ and Ar⁺. At low pressures, T_e is high (see Fig. 3), and the ionization of argon is favored since the ionization rate coefficient of Ar is larger than that of O for $T_e > 2.5$ eV. At higher pressures, T_e is lower, and the generation of O⁺ is favored; in addition, asymmetric charge
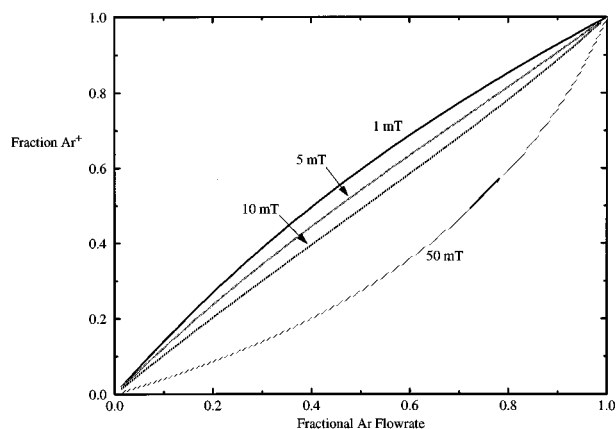
FIG. 10. Fraction of Ar$^+$ vs fraction of argon in the feed gas. Absorbed power=1000 W, total flowrate=35 sccm, γ_{rec}=0.0.

exchange between Ar$^+$/O and Ar$^+$/O$_2$ also destroys argon ions, which further decreases the Ar$^+$ density at high pressures. We did not include O$_2^+$ in this comparison because the O$_2^+$ density is much lower than that of O$^+$.

The effect of argon addition on the concentration of O atoms has also been investigated. The fraction of O atoms plotted in Fig. 11 is defined as the ratio of the O atom density to the total neutral density. The results show that the fraction is nearly independent of pressure, since both the O atom density ([O]) and the total neutral density are nearly linearly dependent on pressure. The enhancement in [O] due to argon addition over that due to the dilution of the feed gas can be attributed to the changes in the electron temperature, which in turn affect the generation and loss rates associated with the oxygen atom.

The total positive-ion density is also enhanced by the addition of argon. At low flows of argon into the system, the behavior of n_+ with pressure follows the trends of an oxygen discharge, (see Fig. 4), where n_+ peaks at approximately 10 mTorr, and decreases at higher pressures. At higher flowrates of argon, i.e., f_{Ar}>0.8, n_+ follows the trends of an argon discharge, where the ion density increases monotonically with increasing pressure. Another parameter of interest is the electronegativity of the discharge. The ratio of n_-/n_e was
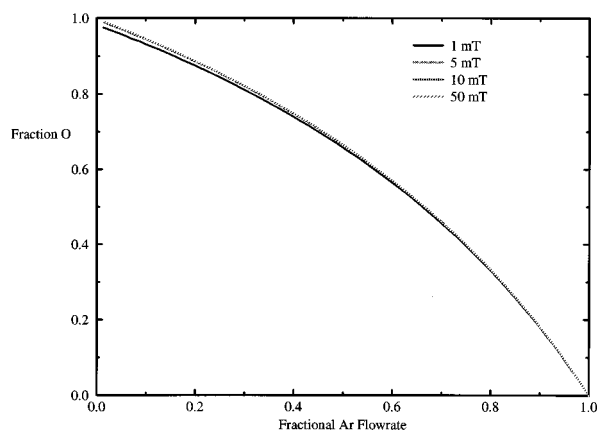
observed to decrease with addition of argon, since the source for negative-ion generation (O$_2$) is reduced, and the presence of Ar$^+$ provides an additional loss mechanism for negative ions through ion–ion recombination.

IV. CONCLUSIONS

We have developed a generalized power balance equation for high-density plasma discharges that can be easily extended to include gas mixtures and polyatomic gases. The equation was used to study discharges of Cl$_2$, O$_2$, and Ar/O$_2$ mixtures. We found that for molecular gases, the electron temperature T_e is no longer a function of pressure and the reactor geometry, but also strongly depends on the plasma composition. The difference in the energy loss channels for each feed gas leads to differences in plasma variables such as ion density, electron temperature, and plasma composition.

We studied the plasma chemistry of molecular gases and their mixtures in a high-density discharge. Fractional dissociations of Cl$_2$ and O$_2$ under normal operating conditions of TCP reactors were shown to be essentially unity when surface recombination processes were not included. When surface reactions were added to the model, we found that the chlorine discharge was more sensitive to surface recombination rate than oxygen. The surface recombination coefficient for chlorine can be as high as 0.15; this high probability of surface recombination can increase the electronegativity of the discharge by increasing the molecular gas concentration, and hence decreasing the fractional dissociation. For an oxygen discharge, the situation is different because the surface recombination rates are slow. In addition, the attachment coefficient for the formation of O$^-$ is smaller than for Cl$^-$, hence, the electronegativity in an O$_2$ discharge is lower than that of a Cl$_2$ discharge under the same operating conditions.

For Ar/O$_2$ mixtures, we found that at low pressures, the dominant ion in the argon-oxygen mixture is Ar$^+$; at higher pressures, however, the dominant ionic species switches to O$^+$. The addition of argon changes the electron temperature of the system, which directly affects the rate coefficients. Since the rate coefficients are strong functions of T_e, we see an increase in the concentration of O atoms in the discharge. The overall positive-ion density was observed to increase as argon flowrate is increased, and the electronegativity of the system decreases as a direct result of the increase in positive-ion density, which increases the volume loss rate of negative ions.

FIG. 11. Fraction of O atom density vs fraction of argon in the feed gas. Absorbed power=1000 W, total flowrate=35 sccm, γ_{rec}=0.0.

APPENDIX

Equations (13) and (14) are modified versions of the equations derived by Godyak and Maximov (see Godyak[36]) and by Lichtenberg *et al.*[37] For a plane parallel discharge, Godyak and Maximov have determined the ratio of sheath edge to center ion density, n_s/n_0,

$$h_{L0} = \frac{0.86}{(3 + L/2\lambda)^{1/2}}. \qquad (A1)$$

For an infinitely long cylindrical discharge, they give a similar result,

$$h_{R0} = \frac{0.8}{(4 + R/\lambda)^{1/2}}. \qquad (A2)$$

Here L and R are the chamber length and radius, and λ is the ion mean-free path. Equations (A1) and (A2) are valid for electropositive discharges in the low to intermediate pressure regime, where $2\lambda/L \geqslant T_i/T_e$ and $\lambda/R \geqslant T_i/T_e$, respectively. For the discharges of interest, Cl_2 in particular, the plasma can become electronegative even at low pressures, especially if the surface recombination coefficient γ_{rec} for generation of Cl_2 from Cl exceeds 0.1. Therefore, we generalize Eqs. (A1) and (A2) to include transitions from electropositive to electronegative regions, and extend the results into the regime of higher pressures.

We use the one-dimensional analytical oxygen model developed by Lichtenberg *et al.*[37] These authors showed that in a plane parallel geometry, with one kind of positive ion and one kind of negative ion, the plasma is composed of three regions: (i) an electronegative (EN) region, where $n_- \gg n_e$, which is confined to the center of the discharge; (ii) two electropositive (EP) regions, with $n_- \ll n_e$, which develop between the EN region and the two sheath edges; and (iii) two thin sheath regions, where $n_+ \gg n_e$ and there are no negative ions. The negative-ion density profile is found to be approximately parabolic, and the relation between the width of the EN region, $2l$, and the chamber length $L = 2l_p$, is found to be

$$l^2 = \frac{2\alpha_0}{\gamma + 2\alpha_0}\left(\frac{2\gamma D l_p}{u_B} + l_p^2\right), \qquad (A3)$$

where α_0 is the ratio of negative ion to electron density at the center of the discharge, n_{-0}/n_{e0}, $\gamma = T_e/T_i$, and $D = eT_i/M_i\nu_i$ is the positive- (and negative) ion diffusion coefficient, with ν_i the ion-neutral collision frequency. The first term in parentheses on the rhs of Eq. (A3) is generally negligible; hence $l \sim l_p$ for $\alpha_0 \gg 1$, and the EN region fills the entire volume, as shown in Fig. 1(c). In this case, the electron density n_e is approximately constant over the entire volume. From the expressions derived by Lichtenberg *et al.*,[37] the sheath edge density can be expressed as a function of α_0, γ, and l_p,

$$n_s = n_{e0}\left(1 + \frac{2\alpha_0}{\gamma}\right)\left(\frac{1}{1 + (l_p u_B/2\gamma D)}\right), \qquad (A4)$$

and from charge neutrality,

$$n_0 = n_{e0}(1 + \alpha_0), \qquad (A5)$$

the h_L factor is found to be

$$h_{L0} = \frac{n_s}{n_0} = \frac{1 + 2\alpha_0/\gamma}{1 + \alpha_0}\frac{1}{1 + (l_p u_B/2\gamma D)}. \qquad (A6)$$

Note that, for electropositive discharges, α_0 is zero, and h_L becomes

$$h_{L0} = \frac{1}{1 + (l_p u_B/2\gamma D)}, \qquad (A7)$$

which is similar to the high-pressure diffusion solution for a plane parallel discharge, with a cosine density distribution. For this system, using the Bohm flux condition at the sheath edge, the h_L factor can be shown to be approximately

$$h_{L0} = \frac{1}{[1 + (2l_p u_B/\pi\gamma D)^2]^{1/2}}. \qquad (A8)$$

Equations (A7) and (A8) are only valid for high pressures, where $l_p u_B/\gamma D \gg 1$. The factor of 2 in Eq. (A7) instead of $\pi/2$ in Eq. (A8) is due to the difference between the parabolic profile assumption and the cosine solution. Heuristically matching Eqs. (A1), (A6), and (A8), we obtained a general h_L factor that can be used for transitions from low to high pressure and from electropositive to electronegative regimes,

$$h_{L0} = \frac{1 + 2\alpha_0/\gamma}{1 + \alpha_0}\frac{0.86}{[3 + (L/2\lambda) + (0.86 L u_B/\pi\gamma D)^2]^{1/2}}, \qquad (A9)$$

where $L = 2l_p$. Since the global model does not include spatial variations, we approximate α_0 as $(3/2)\alpha_{avg}$ from the assumption of the parabolic profile. As shown by Lichtenberg *et al.*,[37] this approximation works well for large values of α_0. For small α_0, the negative-ion density is small and the averaging procedure is not important. In Eq. (A9), the peak ion density n_0 must be modified in order to be consistent with the averaged density determined by the global model. Using the parabolic approximation, $n_0 = (3/2)n_i$, and $\alpha_0 = (3/2)\alpha_{avg}$, we approximate the leading term in Eq. (A9) by

$$\frac{1 + (3\alpha_{avg}/\gamma)}{1 + \alpha_{avg}}.$$

Hence the h_L factor now becomes the ratio of the sheath edge density n_{si} to the average bulk density n_i.

The derivation presented in this section is based on the assumption that there is only one type of positive ions present. For multiple ions, Eq. (A9) is valid if we make the assumption that the ratio of the sheath edge density to the bulk density is independent of the type of ion. A similar treatment can be performed in the radial direction, in which we obtain h_R to be

$$h_R = \frac{n_{si}}{n_i}\bigg|_{\text{radial}} = \frac{1 + (3\alpha_{\text{avg}}/\gamma)}{1 + \alpha_{\text{avg}}} \frac{0.8}{\{4 + (R/\lambda) + [0.8 R u_B / 2.405 J_1(2.405)\gamma D]^2\}^{1/2}}. \tag{A10}$$

We can see that in the limit of an electropositive low-pressure discharge, where α_{avg} and $Ru_B/\gamma D \ll 1$, Eq. (A10) reduces to Eq. (A2), and we get back the expression derived by Godyak and Maximov.

[1]S. K. Park and D. J. Economou, J. Appl. Phys. **68**, 3904 (1988).

[2]M. Meyyappan, J. Appl. Phys. **71**, 2574 (1992).

[3]M. Meyyappan and T. R. Govindan, J. Vac. Sci. Technol. A **10**, 1344 (1992).

[4]M. Meyyappan and T. R. Govindan, IEEE Trans. Plasma Sci. **PS-19**, 122 (1991).

[5]E. S. Aydil and D. J. Economou, J. Electrochem. Soc. **139**, 1396 (1992).

[6]G. L. Rogoff, J. M. Kramer, and R. B. Piejak, IEEE Trans. Plasma Sci. **PS-14**, 103 (1986).

[7]N. L. Bassett and D. J. Economou, J. Appl. Phys. **75**, 1931 (1994).

[8]D. Vender, E. Stoffels, W. W. Stoffels, G. M. W. Kroesen, and F. J. de Hoog, 46th GEC, Montreal, 1993.

[9]E. Stoffels, W. W. Stoffels, D. Vender, G. M. W. Kroesen, and F. J. de Hoog, in Ref. 8.

[10]C. Lee, D. B. Graves, M. A. Lieberman, and D. W. Hess, J. Electrochem. Soc. **141**, 1546 (1994).

[11]M. A. Lieberman and R. A. Gottscho, in *Physics of Thin Films*, edited by M. Francombe and J. Vossen (Academic, New York, 1994), Vol. 18.

[12]R. A. Gottscho, G. R. Scheller, T. Intrator, and D. B. Graves, J. Vac. Sci. Technol. A **6**, 1393 (1988).

[13]G. R. Scheller, R. A. Gottscho, T. Intrator, and D. B. Graves, J. Appl. Phys. **64**, 4384 (1988).

[14]G. R. Scheller, R. A. Gottscho, D. B. Graves, and T. Intrator, J. Appl. Phys. **64**, 598 (1988).

[15]V. A. Ivanov and I. V. Makasyuk, Opt. Spectrosc. (USSR) **72**, 159 (1992).

[16]T. Nakano, N. Sadeghi, and R. A. Gottscho, Appl. Phys. Lett. **58**, 458 (1991).

[17]N. Sadeghi, T. Nakano, D. J. Trevor, and R. A. Gottscho, J. Appl. Phys. **70**, 2552 (1991).

[18]R. B. Bird, W. E. Stewart, and E. N. Lightfoot, *Transport Phenomena* (Wiley, New York, 1960), p. 511.

[19]L. D. B. Kiss and H. H. Sawin, J. Electrochem. Soc. **139**, 1414 (1992).

[20]J. C. Greaves and J. W. Linnett, Trans. Faraday Soc. **55**, 1355 (1959).

[21]J. W. Coburn, J. Vac. Sci. Technol. B **12**, 1417 (1994).

[22]Y. Ra, S. G. Bradley, and C. H. Chen (unpublished).

[23]L. J. Mahoney, A. E. Wendt, E. Barriros, C. J. Richards, and J. L. Shohet (unpublished).

[24]T. Oomori, M. Tuda, H. Ootera, and K. Ono, J. Vac. Sci. Technol. A **9**, 722 (1991).

[25]D. Margreiter, H. Deutsch, and T. D. Mark, Contrib. Plasma Phys. **30**, 487 (1990).

[26]D. Rapp and P. Englander-Golden, J. Chem. Phys. **43**, 1464 (1965).

[27]L. R. Peterson and J. E. Allen, Jr., J. Chem. Phys. **56**, 6068 (1972).

[28]C. Rebrion, B. R. Rowe, and J. B. Marquette, J. Chem. Phys. **91**, 6142 (1989).

[29]I. Dotan and A. A. Viggiano, Chem. Phys. Lett. **209**, 67 (1993).

[30]H. S. W. Massey, Proc. R. Soc. London Ser. A **155**, 472 (1936).

[31]M. A. Lennon, K. L. Bell, H. B. Gilbody, J. G. Hughes, A. E. Kingston, M. J. Murray, and F. J. Smith, J. Phys. Chem. Ref. Data **17**, 1285 (1988).

[32]T. N. Rescigno, Lawrence Livermore National Laboratory (unpublished).

[33]P. S. Ganas, J. Appl. Phys. **63**, 277 (1988).

[34]M. V. Kurepa and D. S. Belie, J. Phys. B **11**, 3719 (1978).

[35]P. C. Cosby and H. Helm, SRI Report, PYU 1147/MP 92-280, 1992.

[36]V. A. Godyak, *Soviet Radio Frequency Discharge Research* (Delphic Associates, Inc., Falls Church, VA, 1986), Chap. 5.

[37]A. J. Lichtenberg, V. Vahedi, M. A. Lieberman, and T. Rognlien, J. Appl. Phys. **75**, 2339 (1994).

[38]C. Rebrion, B. R. Rowe, and J. B. Marquette, J. Chem. Phys. **91**, 6142 (1989).

[39]M. J. J. Kushner, Appl. Phys. **71**, 4173 (1992).